Numerical Modeling of a Viscous Incompressible Fluid Flow in a Channel with a Step

Saeed M. Dubas, Paul Bouthellier, Nihal Siriwardana, and Laura Wieserman

1 Introduction

The problem of steady incompressible flow of gases and liquids in a channel with a step has been the subject of many studies in computational fluid dynamics. Panovko [5] used the method of separation of physical factors to model three-dimensional flow of a viscous fluid in a channel with a step at the Reynolds number $R = 100$. He reported circulatory flow near the step, which decreased in intensity toward the channel outlet. Two benchmark problems that are documented in international workshop proceedings [7, 8] are steady expansion flows and contraction flows in channels with a step. Boger [2] provided a comprehensive review for contraction flows for channels with steps. For the flow into a symmetrical contraction in the form of a step, his experimental data suggest the formation of a "trailing edge" vortex downstream of the step, and detecting this vortex posed a major test for a numerical scheme. Dennis and Smith [9] used a method based on central differences, but were unable to detect the trailing edge vortex visually downstream of the step. However, through grid refinement, they were able to infer qualitatively the presence of this vortex. Their results have been supported experimentally by Durst and Loy [10]. Hawken et al. [6] used a Taylor–Galerkin algorithm and were able to visually detect the trailing edge vortex at the Reynolds number $R = 450$. They went up to Reynolds

S. M. Dubas (✉) · L. Wieserman
Engineering and Computer Science Division, University of Pittsburgh at Johnstown, Johnstown, PA, USA
e-mail: dubasis@pitt.edu

P. Bouthellier
Department of Mathematics, University of Pittsburgh at Greensburg, Greensburg, PA, USA

N. Siriwardana
Department of Mathematics, Prairie View A & M University, Prairie View, TX, USA

H. R. Arabnia et al. (eds.), *Advances in Parallel & Distributed Processing, and Applications*, Transactions on Computational Science and Computational Intelligence, https://doi.org/10.1007/978-3-030-69984-0_15

number $R = 100$ for the expansion case and $R = 800$ for the contraction case. We obtained converged results up to Reynolds number $R = 1000$.

This chapter uses a stable fourth-order central difference method [4] by writing Taylor's series expansions of the error terms in a form that produces strong central coefficients.

Our work supports experimental evidence, suggested by Boger [2], that a trailing edge vortex is formed downstream of the step, which can be seen in our plotted stream functions at $R = 200$ to $R = 400$, and later at $R = 1000$. Onur and Baydar [1] carried out experimental work on this problem, and showed photographs for $R = 200$, which are in agreement with our results. Our results are also in good agreement with the tabulated results of Greenspan [3], requiring a relatively coarse grid for the same accuracy.

2 Mathematical Problem

Consider the flow of a viscous incompressible fluid in a channel with a step. The flow is governed by the steady-state Navier–Stokes equations defined by

$$\Delta\psi = -\omega \tag{1}$$

$$\Delta\omega + R\left(\psi_x\omega_y - \psi_y\omega_x\right) = 0 \tag{2}$$

These equations are valid in the interior of the domain in Fig. 1, where ψ and ω are the stream and the vorticity functions respectively, and R is a flow parameter called the Reynolds number. The boundary conditions to be satisfied are

$$\psi = 1, \quad \psi_y = 0, \quad \text{on} \quad \text{HG} \tag{3}$$

$$\psi = 0, \quad \psi_y = 0, \quad \text{on} \quad \text{AB, CD, EF} \tag{4}$$

$$\psi = 0, \quad \psi_x = 0, \quad \text{on} \quad \text{BC, DE} \tag{5}$$

$$\psi = 3y^2 - 2y^3, \quad \omega = 12y - 6, \quad \text{on} \quad \text{AH} \tag{6}$$

$$\psi_x = 0, \quad \omega_x + R\psi_y\left(\omega + \psi_{yy}\right) = 0 \ \text{ on } \ \text{FG} \tag{7}$$

Conditions (6) are those of Poiseulle flow, while conditions (7) make the flow horizontal and the pressure constant on FG.

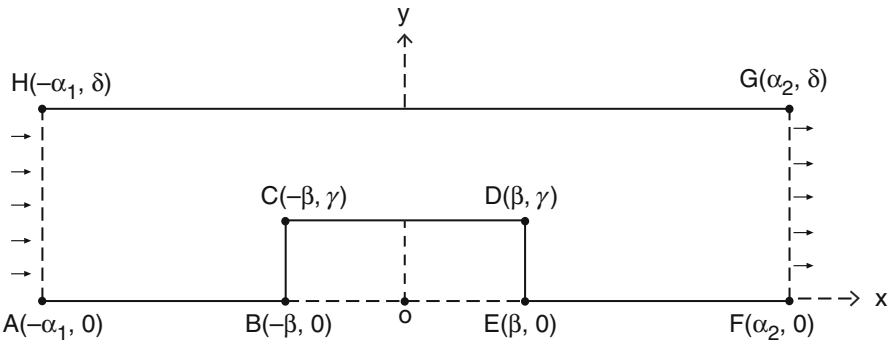

Fig. 1 The channel with a step

Fig. 2 The grid

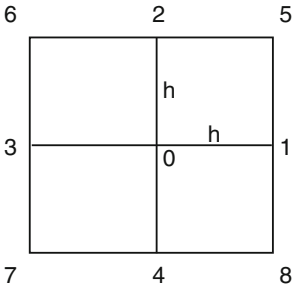

3 The Difference Schemes

We present the difference methods for the given differential equations (1)–(2) as a special case of the second-order elliptic equation.

$$Lu \equiv u_{xx} + u_{yy} + p\,(x,\,y)\,\psi_x + q\,(x,\,y)\,u_y + r\,(x,\,y)\,u = s\,(x,\,y) \tag{8}$$

Note that since $r(x, y) = 0$ for both (1) and (2), we may write (8) as

$$Lu \equiv u_{xx} + u_{yy} + pu_x + qu_y = s \tag{9}$$

where $p = p(x, y)$, $q = q(x, y)$, and $s = s(x, y)$.

Also, note that

$p(x, y) = q(x, y) = 0$, $\quad s(x, y) = -\omega$ for (1),

$p(x, y) = -R\psi_y$, $q(x, y) = R\psi_x$, $s(x, y) = 0$ for (2).

Using the grid shown in Fig. 2, which shows the placement of nine points, we obtain the following approximations at the point (x_i, y_j), numbered 0 in Fig. 2.

$$u_{xx} = \frac{u_3 - 2u_0 + u_1}{h^2} - \frac{h^2}{12}u_{xxxx} + O\left(h^4\right) \tag{10}$$

$$u_{yy} = \frac{u_4 - 2u_0 + u_{21}}{h^2} - \frac{h^2}{12}u_{yyyy} + O\left(h^4\right) \tag{11}$$

$$u_x = \frac{u_1 - u_3}{2h} - \frac{h^2}{6}u_{xxx} + O\left(h^4\right) \tag{12}$$

$$u_y = \frac{u_4 - u_2}{2h} - \frac{h^2}{6}u_{xxx} + O\left(h^4\right) \tag{13}$$

Substituting (10)–(13) into the differential Eq. (9), we obtain the difference operator L_h, defined by

$$L_h u_0 \equiv \sum_{i=0}^{4} \alpha_i u_i = s_0 + E_0(u) \tag{14}$$

where $E_0(u)$ is the truncation error given by

$$E_0(u) = \frac{h^2}{12}\left(u_{xxxx} + 2pu_{xxx} + u_{yyyy} + 2pu_{yyy}\right) + O\left(h^4\right) \tag{15}$$

and

$$\begin{aligned} \alpha_0 &= -\frac{4}{h^2} \\ \alpha_1 &= \frac{1}{h^2} + \frac{p_0}{2h} \\ \alpha_2 &= \frac{1}{h^2} + \frac{q_0}{2h} \\ \alpha_3 &= \frac{1}{h^2} - \frac{p_0}{2h} \\ \alpha_4 &= \frac{1}{h^2} - \frac{q_0}{2h} \end{aligned} \tag{16}$$

Note that when $p(x, y) = -R\psi_y$ or $q(x, y) = R\psi_x$ is large, that is, when R is large, the central difference coefficient α_0 is small relative to the other coefficients, which is the main cause of instability of the central difference method.

To obtain a stable fourth-order operator, we rewrite the central difference approximation (13) in a form that includes the error terms. Therefore,

$$L_h u_0 - E_0(u) = s_0 \tag{17}$$

We next denote the error term $E_0(u)$ in terms of the lower order derivatives given by (10)–(13), and mixed partial derivatives $u_{xy,}$ etc., which can be denoted by the nine points grid in Fig. 2, with a stabilizing effect. From (9), we have

$$u_{xx} = -\left(pu_x + qu_y - u_{yy}\right) + s \tag{18}$$

Differentiating both sides of this equation with respect to x to obtain u_{xxx} and u_{xxxx}, we have

$$\begin{aligned} u_{xxxx} + 2pu_{xxx} = -\Big[&\left(p^2 + 2p_x\right) u_{xx} + \left(pp_x + p_{xx}\right) u_x \\ &+ \left(pq_x + q_{xx}\right) u_y + \left(pq + 2q_x\right) u_{yx} + pu_{yyx} + qu_{yxx} \\ &+ u_{yyxx}\Big] + ps_x + s_{xx} \end{aligned} \tag{19}$$

Similarly, we have

$$\begin{aligned} u_{yyyy} + 2qu_{yyy} = -\Big[&\left(q^2 + 2q_y\right) u_{yy} + \left(qq_y + q_{yy}\right) u_y \\ &+ \left(qp_y + p_{yy}\right) u_x + \left(pq + 2p_y\right) u_{xy} + qu_{xxyy} + pu_{xyy} \\ &+ u_{xxyy}\Big] + qs_y + s_{yy} \end{aligned} \tag{20}$$

Substituting (19) and (20) into (15), we have

$$\begin{aligned} E_0(u) = -\tfrac{h^2}{12} \Big[&\left(p^2 + 2p_x\right) u_{xx} + \left(pp_x + qp_y + p_{xx} + p_{yy}\right) u_x \\ &+ \left(q^2 + 2q_y\right) u_{yy} + \left(pq_x + qq_y + q_{xx} + q_{yy}\right) u_y \\ &+ 2\left(pq + p_y + q_x\right) u_{xy} + 2\left(pu_{xyy} + qu_{xxy} + u_{xxyy}\right) \\ &+ \tfrac{h^2}{12}\left(ps_x + qs_y + s_{xx} + s_{yy}\right) u_y + O\left(h^4\right) \end{aligned} \tag{21}$$

Note that the terms $(p^2 + 2p_x)u_{xx}$ and $(q^2 + 2q_y)u_{yy}$ can produce strong central coefficients when approximated by (10) and (11).

Substituting (21) into (17), we obtain

$$L_h u_0 - \overline{E}_0(u) = s_0^* \tag{22}$$

where

$$\overline{E}_0(u) = E_0(u) - \frac{h^2}{12}\left(ps_x + qs_y + s_{xx} + s_{yy}\right) \tag{23}$$

and

$$s_0^* = s_0 + \frac{h^2}{12}\left(ps_x + qs_y + s_{xx} + s_{yy}\right) \tag{24}$$

We approximate $\overline{E}_0(u)$ using (10)–(13), whereas the mixed partial derivatives u_{xy}, u_{xxy}, u_{yyx}, u_{xxyy} can be readily approximated using Taylor series expansion at the nine point grid, which leads to

$$\overline{E}_0(u) = \sum_{i=0}^{8} \beta_i u_i + O\left(h^4\right) \tag{25}$$

where

$$\begin{aligned}
\beta_0 &= -\frac{4}{6h^2} + \frac{1}{6}\left(p^2 + q^2 + 2p_x + 2q_y\right)\\
\beta_1 &= \frac{2}{6h^2} + \frac{p_0}{6h} - \frac{1}{12}\left(p^2 + 2p_x\right) - \frac{h}{24}\left(pp_x + qp_y + p_{xx} + p_{yy}\right)\\
\beta_2 &= \frac{2}{6h^2} + \frac{q_0}{6h} - \frac{1}{12}\left(q^2 + 2q_y\right) - \frac{h}{24}\left(pq_x + qq_y + q_{xx} + q_{yy}\right)\\
\beta_3 &= \frac{2}{6h^2} - \frac{p_0}{6h} - \frac{1}{12}\left(p^2 + 2p_x\right) + \frac{h}{24}\left(pp_x + qp_y + p_{xx} + p_{yy}\right)\\
\beta_4 &= \frac{2}{6h^2} - \frac{q_0}{6h} - \frac{1}{12}\left(q^2 + 2q_y\right) + \frac{h}{24}\left(pq_x + qq_y + q_{xx} + q_{yy}\right)\\
\beta_5 &= \frac{-1}{6h^2} - \frac{p_0 + q_0}{12h} - \frac{pq + p_y + q_x}{24}\\
\beta_6 &= \frac{-1}{6h^2} + \frac{q_0 - p_0}{12h} + \frac{pq + p_y + q_x}{24}\\
\beta_7 &= \frac{-1}{6h^2} - \frac{p_0 - q_0}{12h} - \frac{pq + p_y + q_x}{24}\\
\beta_8 &= \frac{-1}{6h^2} + \frac{q_0 - p_0}{12h} + \frac{pq + p_y + q_x}{24}
\end{aligned} \tag{26}$$

Substituting (25) into (22), we obtain a stable fourth-order operator L_h^* for (9), defined by

$$L_h^* u_0 \equiv \sum_{i=0}^{4} u_i^* = s_0^* + E_0^*(u) \tag{27}$$

where

$$\begin{aligned}
E_0^*(u) = h^4\Big[&\frac{p^2 u_{xxxx}(\zeta_1,\eta_1) + q^2 u_{yyyy}(\zeta_2,\eta_2)}{144}\\
&+ 2pqh^4\left(u_{xxxy}(\zeta_3,\eta_3) + u_{xyyy}(\zeta_4,\eta_4)\right)\Big]
\end{aligned} \tag{28}$$

and s_0^* is given by (24), and $\alpha_i^* = \alpha_i - \beta_i$.

We also see that the local truncation error $E_0^*(u)$ is $O(h^4)$.

We now set up the difference equations for (1) and (2). For (1), $p = q = 0$ and $s = -\omega$, which leads to the following difference equation

$$L_h^* \psi_0 \equiv \sum_{i=0}^{4} \alpha_i^* \psi_i = s_0^* + E_0^*(u) \tag{29}$$

where

$$\begin{aligned} \alpha_0^* &= -\tfrac{20}{6h^2} \\ \alpha_1^* &= \alpha_2^* = \alpha_3^* = \alpha_4^* = \tfrac{4}{6h^2} \\ \alpha_5^* &= \alpha_6^* = \alpha_7^* = \alpha_8^* = \tfrac{1}{6h^2} \end{aligned} \tag{30}$$

and

$$s_0^* = -\omega_0 - \frac{h^2}{12}\left(\omega_{xx} + \omega_{yy}\right) \tag{31}$$

Next, for (2), $p = -R\psi_y$, $\quad q = R\psi_x$, and $s = 0$, which results in the following difference equation

$$L_h^* \omega_0 \equiv \sum_{i=0}^{4} \alpha_i^* \omega_i = s_0^* + E_0^*(u) \tag{32}$$

where

$$\begin{aligned} \alpha_0 &= -\frac{20}{6h^2} - \frac{1}{6}\left(p^2 + q^2 + 2p_x + 2q_y\right) \\ \alpha_1 &= \frac{4}{6h^2} + \frac{p_0}{3h} + \frac{1}{12}\left(p^2 + 2p_x\right) + \frac{h}{24}\left(pp_x + qp_y + p_{xx} + p_{yy}\right) \\ \alpha_2 &= \frac{4}{6h^2} + \frac{q_0}{3h} + \frac{1}{12}\left(q^2 + 2q_y\right) + \frac{h}{24}\left(pq_x + qq_y + q_{xx} + q_{yy}\right) \\ \alpha_3 &= \frac{4}{6h^2} - \frac{p_0}{3h} + \frac{1}{12}\left(p^2 + 2p_x\right) - \frac{h}{24}\left(pp_x + qp_y + p_{xx} + p_{yy}\right) \\ \alpha_4 &= \frac{4}{6h^2} - \frac{q_0}{3h} + \frac{1}{12}\left(q^2 + 2q_y\right) - \frac{h}{24}\left(pq_x + qq_y + q_{xx} + q_{yy}\right) \\ \alpha_5 &= \frac{1}{6h^2} + \frac{p_0 + q_0}{12h} + \frac{pq + p_y + q_x}{24} \\ \alpha_6 &= \frac{1}{6h^2} + \frac{q_0 - p_0}{12h} - \frac{pq + p_y + q_x}{24} \\ \alpha_7 &= \frac{1}{6h^2} - \frac{p_0 + q_0}{12h} + \frac{pq + p_y + q_x}{24} \\ \alpha_8 &= \frac{1}{6h^2} - \frac{q_0 - p_0}{12h} - \frac{pq + p_y + q_x}{24} \end{aligned} \tag{33}$$

4 Comparison of Results

We ran the present scheme and the scheme of Greenspan [3] at each of the indicated points $(x, y) = (0.1, 0.1)$, and $(x, y) = (1.9, 0.8)$ for ψ and ω, $\alpha_1 = \alpha_2 = 4$, $\gamma = 0.5$, $\delta = 1$, various values of the step size h and Reynolds number R. To check the efficiency, we compared the results at the same points for both methods, as given by Tables 1A, 1B, 2A, 2B, 3A, and 3B.

Table 1A Stream values at $R = 50$

Present (0.1,0.1)		Greenspan (0.1,0.1)	Present (1.9,0.8)	Greenspan (1.9,0.8)
R	Ψ	Ψ	Ψ	Ψ
$h = 0.1$	2.780 E-02	2.841 E-02	0.8812	0.8775
$h = 0.05$	2.797 E-02	2.813 E-02	0.8825	0.8815
$h = 0.025$	2.797 E-02	2.802 E-02	0.8829	0.8824
$h = 0.0125$	2.797 E-02	2.798 E-02	0.8831	0.8829
$h = 0.00625$	2.797 E-02	2.798 E-02	0.8831	0.8830

Table 1B Vorticity values at $R = 50$

Present (0.1,0.1)		Greenspan (0.1,0.1)	Present(1.9,0.8)	Greenspan (1.9,0.8)
R	ω	ω	ω	ω
$h = 0.1$	−48E-01	−4732 E-01	3567 E-01	3529 E-01
$h = 0.05$	−4798 E-01	−4776 E-01	3609 E-01	3593 E-01
$h = 0.025$	−4798 E-01	−4792 E-01	3610 E-01	3608 E-01
$h = 0.0125$	−4799 E-01	−4797 E-01	3611 E-01	3612 E-01
$h = 0.00625$	−4799 E-01	−4799 E-01	3612 E-01	3611 E-01

Table 2A Stream values at $R = 100$

Present (0.1,0.1)		Greenspan (0.1,0.1)	Present(1.9,0.8)	Greenspan (1.9,0.8)
R	Ψ	Ψ	Ψ	Ψ
$h = 0.1$	2.8 E-02	2.822 E-02	0.8765	0.8801
$h = 0.05$	2.794 E-02	2.805 E-02	0.8772	0.8757
$h = 0.025$	2.794 E-02	2.797 E-02	0.8777	0.8772
$h = 0.0125$	2.794 E-02	2.795 E-02	0.8779	0.8776
$h = 0.00625$	2.794 E-02	2.794 E-02	0.8780	0.8778

Table 2B Vorticity values at $R = 100$

Present (0.1,0.1)		Greenspan (0.1,0.1)	Present(1.9,0.8)	Greenspan (1.9,0.8)
R	ω	ω	ω	ω
$h = 0.1$	-48E-01	−4749 E-01	3495 E-01	3417 E-01
$h = 0.05$	−4797 E-01	−4782 E-01	3510 E-01	3494 E-01
$h = 0.025$	−4799 E-01	−4794 E-01	3516 E-01	3512 E-01
$h = 0.0125$	−4799 E-01	−4798 E-01	3517 E-01	3517 E-01
$h = 0.00625$	−4799 E-01	−4799 E-01	3519 E-01	3518 E-01

Table 3A Stream values at $R = 1000$

Present (0.1,0.1)		Greenspan (0.1,0.1)	Present(1.9,0.8)	Greenspan (1.9,0.8)
R	Ψ	Ψ	Ψ	Ψ
$h = 0.1$	2.730 E-02	2.727 E-02	0.8594	0.8412
$h = 0.05$	2.768 E-02	2.750 E-02	0.8477	0.8403
$h = 0.025$	2.762 E-02	2.758 E-02	0.8539	0.8539
$h = 0.0125$	2.760 E-02	2.760 E-02	0.8542	0.8549
$h = 0.00625$	2.760 E-02	2.760 E-02	0.8545	0.8549

Table 3B Vorticity values at $R = 1000$

Present (0.1,0.1)		Greenspan (0.1,0.1)	Present(1.9,0.8)	Greenspan (1.9,0.8)
R	ω	ω	ω	ω
$h = 0.1$	−4716 E-01	−4799 E-01	5733 E-01	2956 E-01
$h = 0.05$	−4793 E-01	−4808 E-01	3105E-01	3064 E-01
$h = 0.025$	−4806 E-01	−4809 E-01	3114 E-01	3109 E-01
$h = 0.0125$	−4808 E-01	−4809E-01	3116E-01	3122E-01
$h = 0.00625$	−4808 E-01	−4809 E-01	3120 E-01	3124 E-01

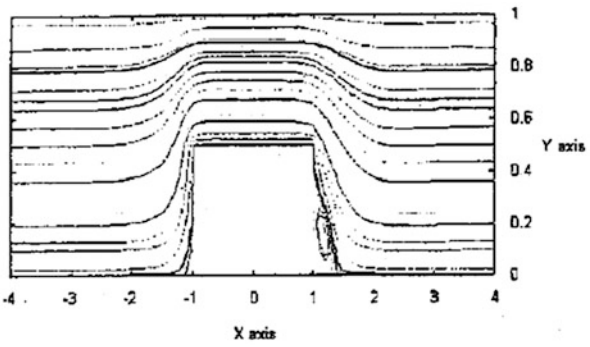

Fig. 3 Plot of ψ for $h = 0.1$, $R = 10$

Results of both methods converged, but for the stream function at $R = 50$ and $R = 1000$, we obtained four digit accuracy for $h = 0.05$, whereas Greenspan scheme required $h = 0.00625$ for the same accuracy.

At $R = 1000$, we obtained four digit accuracy at step size $h = 0.05$, whereas the Greenspan's scheme required $h = 0.00125$ for the same accuracy.

Using the data obtained from the present scheme, the stream curves are plotted in Figs. 3, 4, 5, 6, 7, 8, 9, 10, 11, 12, 13, and 14, whereas vorticity curves are plotted in Figs. 15, 16, 17, and 18.

From the graphs, we can see that the role of the step size is limited for lower values of R, like $R = 10$ and $R = 50$ in Figs. 3 and 4, but when the value of R becomes 100 or 1000, the step size plays an important role, which is obvious from Figs. 9 and 10, where there is a counterflow on the left-hand side of the channel when step size $h = 0.025$. However, for larger values of h, there is no counterflow on the left-hand side of the channel for the same value of $R = 100$ (see Figs. 7 and 8).

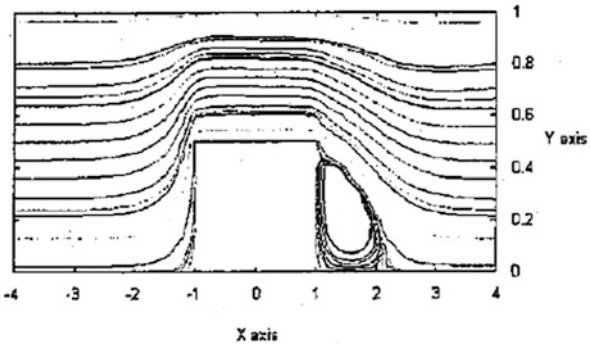

Fig. 4 Plot of ψ for $h = 0.1$, $R = 50$

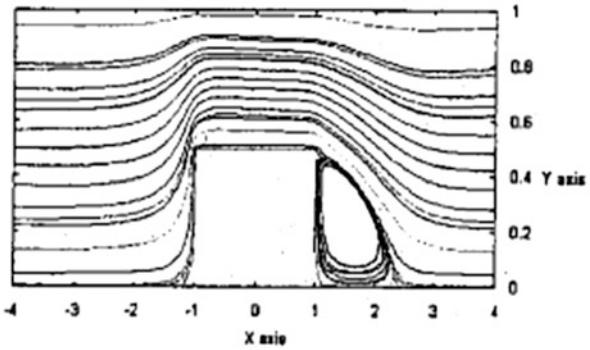

Fig. 5 Plot of ψ for $h = 0.05$, $R = 50$

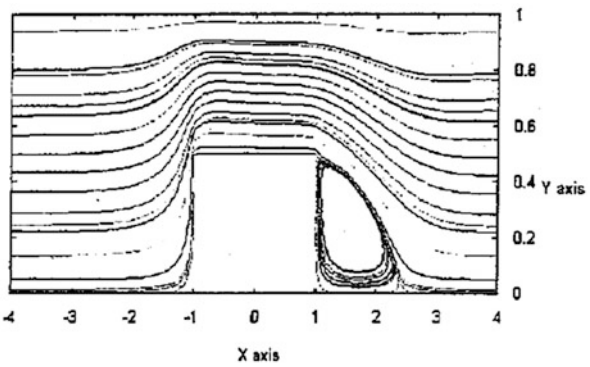

Fig. 6 Plot of ψ for $h = 0.025$, $R = 50$

In the present scheme, counterflow to the left-hand side of the channel appears for the first time when $R = 100$ and the step size is as small as $h = 0.025$, as shown in Fig. 9. Onur and Baydar [1] did experimental work on this problem and showed photographs for $R = 200$. Our results are in agreement with those photographs. Experimental evidence presented by Boger [2] suggests that a trailing edge vortex is formed downstream of the step, which can be seen in our plotted stream functions for $R = 200$, 300, 400, and $h = 0.0125$ in Figs. 13, 14, and 15. It can also be seen in the $R = 1000$ case, see Fig. 10.

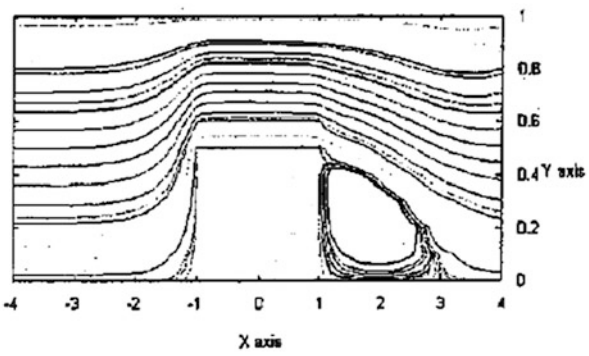

Fig. 7 Plot of ψ for $h = 0.1$, $R = 100$

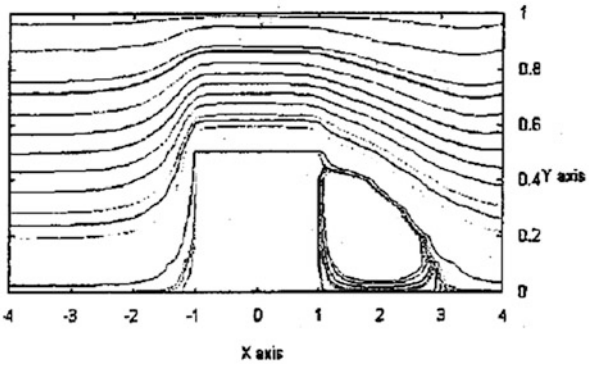

Fig. 8 Plot of ψ for $h = 0.05$, $R = 100$

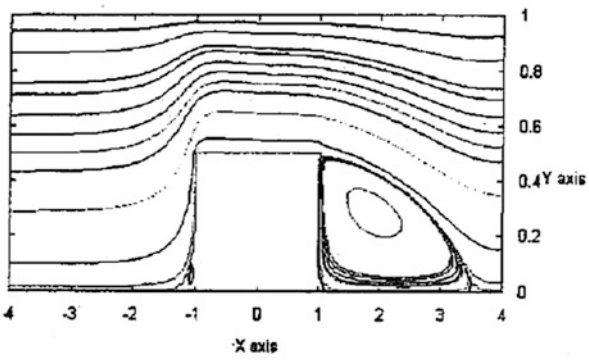

Fig. 9 Plot of ψ for $h = 0.025$, $R = 100$

4.1 Effect of Step Height on the Flow

We checked the effect of varying the step height on the flow, where D denotes the height of the channel at the step ($D < 1$, maximum height).

When $D = 0.25$, it can be seen from the graph in Fig. 11 that flow is everywhere in the channel. There is a large counterflow on the right-hand side and a small counter flow on the left-hand side of the step as compared to the standard case when

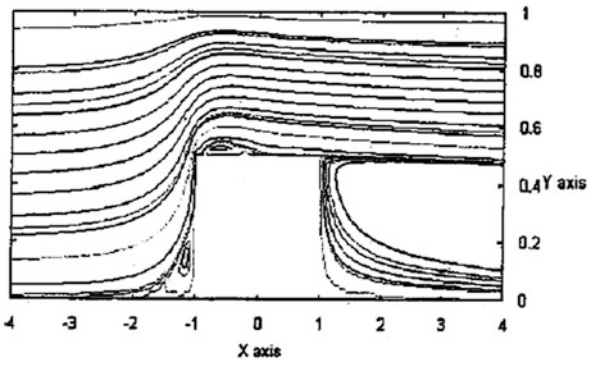

Fig. 10 Plot of ψ for $h = 0.025$, $R = 1000$

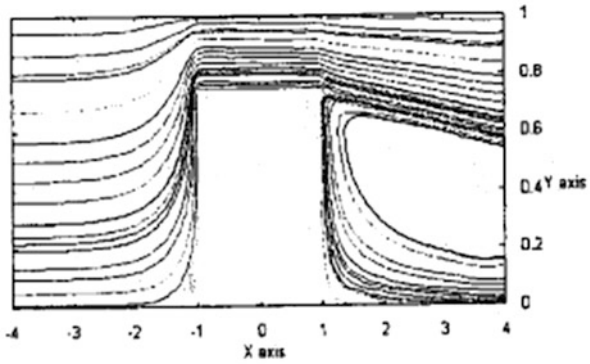

Fig. 11 Plot of ψ for $h = 0.05$, $D = 0.25$, $R = 100$

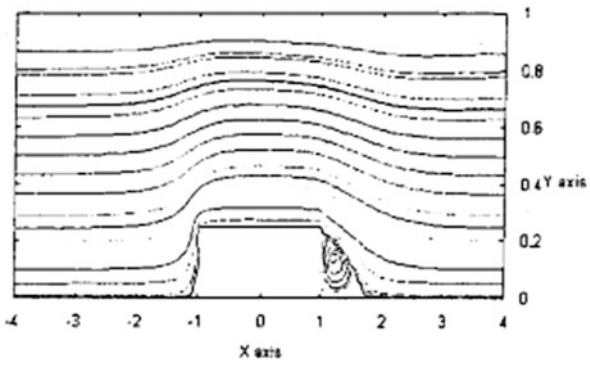

Fig. 12 Plot of ψ for $h = 0.05$, $D = 0.75$, $R = 100$

$D = 0.5$, where there is a small counter flow on the right-hand side and no counter flow on the left-hand side of the step, as seen from Fig. 8.

On increasing the value of D to 0.75, as in Fig. 12, flow can be seen everywhere in the channel. There is a small counterflow on the right-hand side of the step as compared to the standard case when $D = 0.5$. Also, refer to Fig. 19 for other interesting results.

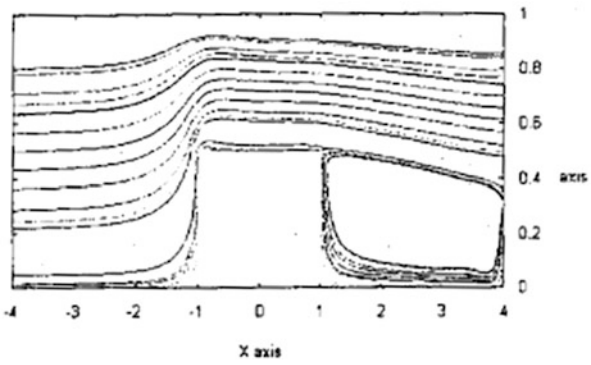

Fig. 13 Plot of ψ for $h = 0.0125$, $R = 200$

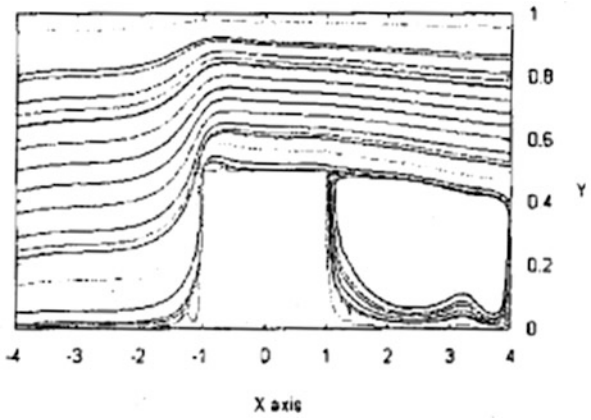

Fig. 14 Plot of ψ for $h = 0.0125$, $R = 300$

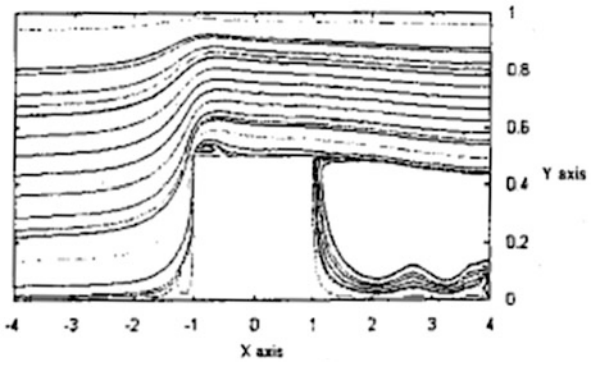

Fig. 15 Plot of ψ for $h = 0.0125$, $R = 400$

5 Conclusion

In this chapter, we used a high-order numerical scheme based on Choo and Schultz's work [4] to study the flow of a viscous incompressible fluid in a channel with a step. The numerical scheme expressed the error terms of the central difference method in

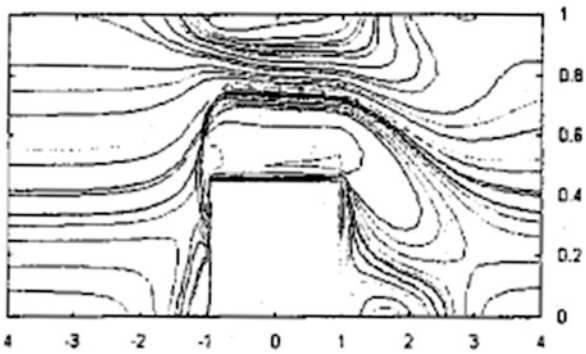

Fig. 16 Plot of ω for $h = 0.05$, $R = 50$

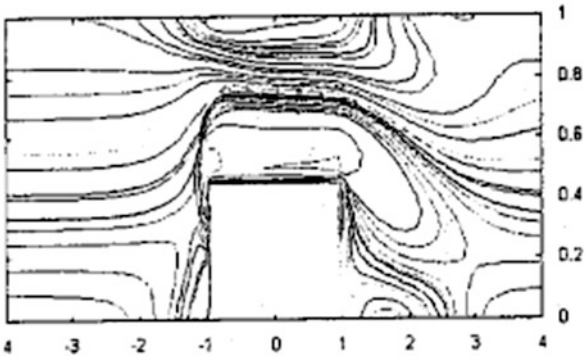

Fig. 17 Plot of ω for $h = 0.05$, $R = 100$

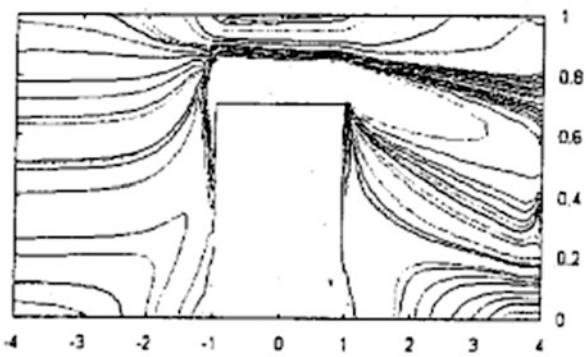

Fig. 18 Plot of ω for $h = 0.05$, $D = 0.25$, $R = 1000$

such a form that led to a stable fourth-order operator. The results obtained were in good agreement with the experimental, graphical, and tabulated results obtained in other studies.

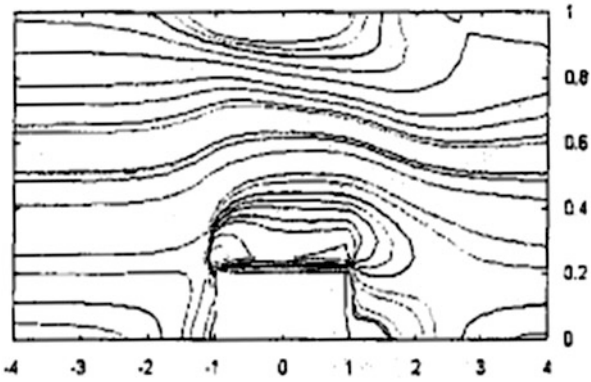

Fig. 19 Plot of ω for $h = 0.05$, $D = 0.75$, $R = 100$

References

1. H.S. Onur, Baydar, Laminar channels flow over a square step. Int. J. Eng. Sci. **30**(9), 1109–1116 (1992)
2. D.V. Boger, Viscoelastic flow through contractions. Ann. Rev. Fluid. Mech., 157–182 (1987)
3. D. Greenspan, Numerical studies of steady, viscous, incompressible flow in a channel with a step. J. Eng. Math. **3**, 21–28 (1969)
4. J.Y. Choo, D. Schultz, A high order difference method for the steady state Navier –Stokes equations. Comput. Math. Applic. **27**(11), 105–119 (1994)
5. M.Y. Panovko, Numerical modelling of three dimensional flows of a viscous incompressible fluid in a channel with a step. translated from Teplofizika Vysokikh Temperetur **27**(6), 1126–1131 (1989)
6. D.M. Hawken, P. Townsend, M.F. Webster, Numerical simulations of viscous flows in channels with a step. J. Comput. Fluids **20**(1), 59–75 (1991)
7. Proc, *6th Mtg of the IAHR Working Group on Refined Modelling of Flows* (Karlsruhe, 1983)
8. K. Morgan, J. Periaux, F. Thomasset (eds.), *Analysis of Laminar Flow Over a Backward Facing Step* (Proc. GAMM Wkshp, Bievres, 1983)
9. S.C.R. Dennis, F.T. Smith, Steady flow through a channel with a symmetrical constriction in the form of a step. Proc. Royal Soc. Lond. **A327**, 393 (1980)
10. F. Durst, T. Loy, Investigations of Laminar flow in a pipe with sudden constriction of cross sectional area. Computers Fluids **13**(1), 15 (1985)